



## Abstract

Particle concentration measurements with underwing probes on aircraft are impacted by air compression upstream of the instrument body as a function of flight velocity. In particular for fast-flying aircraft the necessity arises to account for compression of the air sample volume. Hence, a correction procedure is needed to invert measured particle number concentrations to ambient conditions that is commonly applicable for different instruments to gain comparable results. In the compression region where the detection of particles occurs (i.e. under factual measurement conditions), pressure and temperature of the air sample are increased compared to ambient (undisturbed) conditions in certain distance away from the aircraft. Conventional procedures for scaling the measured number densities to ambient conditions presume that the particle penetration speed through the instruments' detection area equals the aircraft speed (True Air Speed, TAS). However, particle imaging instruments equipped with pitot-tubes measuring the Probe Air Speed (PAS) of each underwing probe reveal PAS values systematically below those of the TAS. We conclude that the deviation between PAS and TAS is mainly caused by the compression of the probed air sample. From measurements during two missions in 2014 with the German Gulfstream G-550 (HALO – High Altitude LOnge range) research aircraft we develop a procedure to correct the measured particle concentration to ambient conditions using a thermodynamic approach. With the provided equation the corresponding concentration correction factor  $\xi$  is applicable to the high frequency measurements of each underwing probe which is equipped with its own air speed sensor (e.g. a pitot-tube).  $\xi$ -values of 1 to 0.85 are calculated for air speeds (i.e. TAS) between 60 and 260  $\text{ms}^{-1}$ . From HALO data it is found that  $\xi$  does not significantly vary between the different deployed instruments. Thus, for the current HALO underwing probe configuration a parameterisation of  $\xi$  as a function of TAS is provided for instances if PAS measurements are lacking. The  $\xi$ -correction yields higher ambient particle concentration by about 15–25 % compared to conventional procedures – an improvement which can be considered as significant for many research

## Thermodynamic approach to correct for compression at Mach 0.7

R. Weigel et al.

Title Page

Abstract

Introduction

Conclusions

References

Tables

Figures



Back

Close

Full Screen / Esc

Printer-friendly Version

Interactive Discussion



applications. The calculated  $\xi$ -values are specifically related to the considered HALO  
underwing probe arrangement and may differ for other aircraft or instrument geometries.  
Moreover, the  $\xi$ -correction may not cover all impacts originating from high flight  
velocities and from interferences between the instruments and, e.g., the aircraft wings  
and/or fuselage. Consequently, it is important that PAS (as a function of TAS) is individually  
measured by each probe deployed underneath the wings of a fast-flying aircraft.

## 1 Introduction

Clouds constitute one of the most important regulators of the Earth's energy balance.  
The radiation net effect of various cloud types is not ultimately known yet. The albedo  
effect and the greenhouse effect of clouds are driven by the cloud element's microphysical  
properties (e.g. the particles' number, size and shape). In a first order estimate the  
cloud particle size is mostly determined by the cloud particle number concentration,  
since the available water vapour for condensation is distributed via diffusion over the  
number of particles present within a cloud. Cloud particle number concentrations are  
highly variable (e.g. Krämer et al., 2009), typically ranging between a few thousandths  
and up to hundreds of particles per cubic centimetre, since specific mechanisms of  
cloud formation are determined by local dynamics (e.g. Spichtinger and Gierens, 2009;  
Kärcher and Lohmann, 2002).

Airborne in situ investigations related to the microphysical properties of cloud particles,  
ice crystals, and hydrometeors are essential for answering many scientific questions  
and therefore measurement methods by means of underwing probes are widely used  
(cf. Baumgardner et al., 2011; Wendisch and Brenguier, 2013). Airborne in situ  
measurements of cloud elements are generally influenced by aerodynamic conditions  
at the instrument's individual mounting position, i.e. due to specific flow fields around  
the aircraft's fuselage and wings (Drummond and MacPherson, 1985; Norment and  
Quealy, 1988). Local fluctuations of the air density may occur in the vicinity of  
measurement instruments and their sensing volumes (MacPherson and Baumgardner, 1988)

### Thermodynamic approach to correct for compression at Mach 0.7

R. Weigel et al.

Title Page

Abstract

Introduction

Conclusions

References

Tables

Figures



Back

Close

Full Screen / Esc

Printer-friendly Version

Interactive Discussion



which can affect typical measurements like particle number concentrations and subsequently derived distributions of surface, areas or volumes. Consequently, if possible, the thermodynamic conditions during particle detection need to be considered for gaining accurate and comparable results.

Two scientific missions were carried out in 2014 with the German Gulfstream G-550 (HALO – High Altitude LOnge range), the sister ship of the US research aircraft HIA-PER (High-Performance Instrumented Airborne Platform for Environmental Research), (Laursen et al., 2006): (1) ML-CIRRUS, from 24 March to 30 April, with a total of ~ 71 measurement flight hours at mid-latitudes over Central Europe (Voigt et al., 2015), and (2) ACRIDICON-CHUVA, during September, with overall ~ 96 local mission flight hours in tropical regions, over the Amazonian basin, Brazil (Wendisch et al., 2015). During both missions, several independent underwing probes were deployed (e.g. a Cloud Combination Probe – CCP; a Small Ice Detector – SID3; a Cloud, Aerosol and Precipitation Spectrometer – CAPS; a Cloud and Aerosol Spectrometer – CAS, a Precipitation Imaging Probe – PIP; and the Particle Habit Imaging and Polar Scattering – PHIPS-probe) for studies concerning cloud particle microphysical properties at relative high flight velocities reached by HALO (up to Mach 0.75). Thus, the impact on the air flow conditions towards underwing probes, previously considered numerically for flight velocities between 50 and 130 ms<sup>-1</sup> (Norment and Quealy, 1988) and empirically for up to 100 ms<sup>-1</sup> (MacPherson and Baumgardner, 1988), needs to be re-assessed for the air compression accompanied with high flight velocities.

The diagram in Fig. 1 shows an aircraft fuselage under flight conditions when passing a field of enhanced particle concentration, e.g., a cloud. By means of avionic (meteorological) sensors in the air data boom (cf. Fig. 1b; also referred to as nose boom) the ambient static air pressure ( $p_1$ ) and temperature ( $T_1$ ) are almost undisturbedly measured. The dynamic pressure proportion provided by the aircraft avionic sensors is transferable into the True Air Speed (TAS) according to Bernoulli's law and describes the aircraft velocity relative to the current motion of air.

## Thermodynamic approach to correct for compression at Mach 0.7

R. Weigel et al.

Title Page

Abstract

Introduction

Conclusions

References

Tables

Figures

◀

▶

◀

▶

Back

Close

Full Screen / Esc

Printer-friendly Version

Interactive Discussion





## Thermodynamic approach to correct for compression at Mach 0.7

R. Weigel et al.

Title Page

Abstract

Introduction

Conclusions

References

Tables

Figures

◀

▶

◀

▶

Back

Close

Full Screen / Esc

Printer-friendly Version

Interactive Discussion



vary for the different instruments, the aircraft type and the position of the probe relative to the aircraft wings and/or fuselage. However, if the instrument is not equipped with a pitot-tube, or the pitot-tube is inoperative, the air speed at the point of measurement is unknown. In such a case the herein provided parameterisation of the compression correction serves as a guideline for adopting the TAS from the aircraft data after adjustments. In the following the application of both, the derived thermodynamic correction and the unadjusted aircraft TAS on a data set of atmospheric measurements, illustrates the sensitivity of the results to the employed procedure. Furthermore, we show that the thermodynamic correction is relatively insensitive to the instrument position with respect to the aircraft fuselage, and the correlations of instrument-specific correction factors demonstrate robustness and consistency of the suggested approach.

## 2 Method

In this section, we describe a new method for determining the number concentration of particles in a given air volume from measured quantities and from basic thermodynamics. We will particularly emphasise the difference between our approach and the conventionally used methods which focus exclusively on geometrical considerations, but neglects effects of air compression.

For the following examination some definitions need to be particularly introduced: All velocities that are specified as air speeds ( $v_1$ ,  $v_2$ , TAS, PAS) and the velocities of particles ( $v_p$ ) refer to the moving aircraft or instruments relative to the air as the reference system. Measurement conditions are those under which the measurement occurs in the detection region that is impacted by compression. Ambient (undisturbed) conditions relate to the initial state far away from the aircraft.

## 2.1 Ambient vs. measured particle number densities

The measured number concentration  $N_{\text{meas}}$  (in units of number per air volume) detected with underwing probes that have a free stream detection volume is defined as:

$$N_{\text{meas}} = n \cdot \frac{1}{A_s \cdot v_p} \cdot \frac{1}{\Delta t} = \frac{n}{V_{\text{meas}}} \quad (1)$$

5 Here,  $n$  denotes the number of particles detected during the time interval  $\Delta t$  (in s), and  $v_p$  denotes the velocity (in  $\text{ms}^{-1}$ ) of particles penetrating the sample area  $A_s$  (in  $\text{m}^2$ ).

In good approximation it can be assumed that  $v_p \approx \text{PAS} = v_2$ . The detection volume is therefore defined as:

$$10 \quad V_{\text{meas}} = A_s \cdot v_2 \cdot \Delta t. \quad (2)$$

The ambient particle number concentration in the undisturbed ambient air is given as:

$$N_{\text{amb}} = \frac{n_{\text{amb}}}{V_1} \quad (3)$$

with the number of particles  $n_{\text{amb}}$  and the ambient air volume  $V_1$  (in  $\text{m}^3$ ).

15 Due to the compression of air upstream of the instruments, the ambient volume  $V_1$  converts into the volume  $V_2$ . Under the presumptions that the particle number per mass  $M$  of the air sample is not affected by compression (i.e. remains constant and thus:  $\frac{n_{\text{amb}}}{M} = \frac{n_{\text{meas}}}{M}$ ), that the particles' inertia is negligible for given streamlines, and that the ideal gas law ( $p \cdot V = M \cdot R_s \cdot T$ ; with  $[p] = \text{kg ms}^{-2}$ ,  $[V] = \text{m}^3$ ,  $[M] = \text{kg}$ ,  $[T] = \text{K}$ ) applies and where  $R_s$  denotes the specific gas constant (in  $\text{J kg}^{-1} \text{K}^{-1}$ ; while  $\text{J} = \text{kg m}^2 \text{s}^{-2}$ ) we end up with the following equation:

$$20 \quad \frac{n}{M} = \text{const.} \implies n_{\text{amb}} \frac{R_s \cdot T_1}{\rho_1 \cdot V_1} = n_{\text{meas}} \frac{R_s \cdot T_2}{\rho_2 \cdot V_2} \quad (4)$$

13429

## Thermodynamic approach to correct for compression at Mach 0.7

R. Weigel et al.

Title Page

Abstract

Introduction

Conclusions

References

Tables

Figures

◀

▶

◀

▶

Back

Close

Full Screen / Esc

Printer-friendly Version

Interactive Discussion



Then we can derive the expression for determining the ambient particle number concentration:

$$N_{\text{amb}} \cdot R_s \cdot \frac{T_1}{\rho_1} = N_{\text{meas}} \cdot R_s \cdot \frac{T_2}{\rho_2} \xrightarrow{v_p=v_2} N_{\text{amb}} = N_{\text{meas}} \cdot \frac{\rho_1}{\rho_2} \cdot \frac{T_2}{T_1}. \quad (5)$$

## 2.2 TAS-based particle number concentrations

If the air speed at the probe (PAS,  $v_2$ ) during measurements is unknown, e.g. for the case that the probe is not equipped with a pitot-tube or when a present pitot-tube is frozen, it is common practice to presume the particle speed ( $v_p$ ) to equal the true air speed (TAS,  $v_1$ ) to determine particle number concentrations (cf. Eq. 1).

Equivalent to using the TAS, the same resulting concentration is achieved when alternatively using the velocity ratio  $\frac{\text{PAS}}{\text{TAS}}$  (i.e.  $\frac{v_2}{v_1}$ ) as the factor for multiplication with measured particle number concentration ( $N_{\text{meas}}$ , cf. Eq. 1), i.e.:

$$N_{\text{meas}} \cdot \frac{v_2}{v_1} = \frac{n}{A_s \cdot t \cdot v_2} \cdot \frac{v_2}{v_1} = \frac{n}{A_s \cdot t \cdot v_1}. \quad (6)$$

If pitot-tube measurements of PAS are available, the treatment of resulting  $N_{\text{meas}}$  with the factor  $\frac{\text{PAS}}{\text{TAS}}$  lacks any physical rationale and relies only on the geometrical consideration that  $V_1 \cdot t^{-1} = \text{TAS} \cdot A_s$  and that  $V_2 \cdot t^{-1} = \text{PAS} \cdot A_s$ . Nevertheless, as both procedures yield identical results with the same error level, in the following the use of TAS for determining a particle number concentration is treated synonymously to correcting  $N_{\text{meas}}$  (as defined in Eq. 1) by the factor  $\frac{\text{PAS}}{\text{TAS}}$ .

This approach results in significantly underestimated particle number concentrations with respect to the ambient conditions for following reasons.

1. By presuming  $v_1$  as the speed of particles while penetrating  $A_s$  it is insinuated that a certain number of particles per  $\Delta t$  was detected while probing a linearly enlarged air volume per  $\Delta t$ . Resulting enlargement would describe an expansion

### Thermodynamic approach to correct for compression at Mach 0.7

R. Weigel et al.

Title Page

Abstract

Introduction

Conclusions

References

Tables

Figures

◀

▶

◀

▶

Back

Close

Full Screen / Esc

Printer-friendly Version

Interactive Discussion







data recorded during the complete flight, regardless of the flight altitude or flight speed. Generally, particles with diameter greater than  $50\ \mu\text{m}$  were analysed, mostly 2–5 images in consecutive order before selecting a new measurement period. Occasionally also droplet images were measured ( $\sim 20\%$  of all analysed images) that were singularly present in a particle population that was either dominated by much smaller cloud elements ( $\sim 20\text{--}40\ \mu\text{m}$ ) or by much larger precipitation particles (usually loose, amorphous ice agglomerates of diameter  $> 600\ \mu\text{m}$ ). Figure 4 depicts the result of these analyses. The scatter of the single data points (Fig. 4a) is statistically processed by means of the aspect ratio median with percentiles (10, 25, 75 and 90 %) in particle diameter size bins of  $30\ \mu\text{m}$  (Fig. 4b). Images of particles with diameter smaller than  $100\ \mu\text{m}$  show distortions within 10 % which is synonymous for a  $v_2$ -PAS-deviation of less than 10 % (cf. Fig. 3). For droplets of diameter between 100 and  $250\ \mu\text{m}$  the image aspect ratios increasingly scatter, but the resulting median does not indicate that  $v_2$  deviates from PAS by more than 10 %. Moreover, for the same droplet size range, a  $v_2$ -PAS-deviation of less than 15 % is suggested by 75 % of the data points. The images of particles with diameter larger than  $250\ \mu\text{m}$  exhibit increasing distortion as the image aspect ratios approach values suggesting a  $v_2$ -PAS-deviation of up to 20 %. However, none of the analysed images exhibits an aspect ratio of about 0.75 which should systematically be the case if  $v_2$  was coincident with TAS. The observations provide the hint that the driving forces arising in the flow field upstream of an underwing probe overcome the inertia resistance even of larger cloud elements of diameter  $> 100\ \mu\text{m}$ . This supports the suggestion that the penetration speed of the vast majority of detected particles through an OAP's detection region may be better described by the PAS ( $v_2$ ), rather than by the TAS ( $v_1$ ).

Hence, we conclude that

- a. the compression of air causes a densification of airborne particles in the detection region of the considered instrument,

## Thermodynamic approach to correct for compression at Mach 0.7

R. Weigel et al.

Title Page

Abstract

Introduction

Conclusions

References

Tables

Figures



Back

Close

Full Screen / Esc

Printer-friendly Version

Interactive Discussion



## Thermodynamic approach to correct for compression at Mach 0.7

R. Weigel et al.

Title Page

Abstract

Introduction

Conclusions

References

Tables

Figures

◀

▶

◀

▶

Back

Close

Full Screen / Esc

Printer-friendly Version

Interactive Discussion



- b. the compression is reflected by systematically lower values of  $v_2$  (PAS) compared to  $v_1$  (TAS), exhibiting a discrepancy that is too large to be covered by a 10% uncertainty of measured PAS,
- c. the particles' velocity while passing the instrument sample area is best approximated with  $v_2$ , rather than with  $v_1$ , and
- d. the conventionally applied practice of treating  $N_{\text{meas}}$  with the factor  $\frac{\text{PAS}}{\text{TAS}}$  (geometric approach) is invalid for correcting measured number concentration to ambient conditions,
- e. a method is needed to reasonably correct  $N_{\text{meas}}$  by accounting for the air compression, particularly at high flight velocities, to determine  $N_{\text{amb}}$ .

### 2.3 Correction of $N_{\text{meas}}$ based on thermodynamic considerations

The expression that accounts for the described compression effect is formulated in its general form with Eq. (5). The unknown parameter in this expression is the probe air temperature  $T_2$  that is increased in comparison to ambient air temperature  $T_1$  as a consequence of the compression. The temperature increase is obtainable by using Bernoulli's law together with the ideal gas law and, furthermore, by presuming adiabatic conditions, i.e. the conservation of energy. The derivation emanates from following different conditions which are illustrated in Figure 1 for the air velocity  $v$ , the air pressure  $p$ , the specific enthalpy  $h$  of a uniform system and the gravitational potential  $\phi$ :

condition 1 – at the aircraft's air data boom:  $v_1, p_1, T_1, h_1, \phi_1$

condition 2 – upstream of the probe:  $v_2, p_2, T_2, h_2, \phi_2$

Bernoulli's law for compressible gases and under the presumption of energy conservation reads as:

$$\frac{1}{2}v_1^2 + h_1 = \frac{1}{2}v_2^2 + h_2, \quad (7)$$



the probed air with respect to ambient conditions. Consequently, the resulting squared velocity difference implies the change of the particles' motion in-line with the flight direction due to the compression.

Rearrangement of Eq. (9) leads to:

$$T_2 = T_1 + \Delta T = T_1 + \frac{1}{2 \cdot c_p} (v_1^2 - v_2^2). \quad (10)$$

The specific heat capacity  $c_p$  of air ranges from about 1002.5 to 1006.4  $\frac{\text{J}}{\text{kg}\cdot\text{K}}$  for atmospheric temperature conditions between 180 to 325 K (Dixon, 2007). Accepting an implied uncertainty in the per-mill-range, the product  $2 \cdot c_p$  in Eq. (10) may be replaced by 2008  $\frac{\text{J}}{\text{kg}\cdot\text{K}}$ .

Implying  $T_2$  from Eq. (14) into Eq. (5) leads to the thermodynamic correction of measured particle number concentrations to account for the compression of air upstream of the probe during flight:

$$N_{\text{amb}} = N_{\text{meas}} \cdot \frac{\rho_1}{\rho_2} \cdot \left( 1 + \frac{1}{2008 \frac{\text{J}}{\text{kg}\cdot\text{K}} \cdot T_1} (v_1^2 - v_2^2) \right) = N_{\text{meas}} \cdot \xi. \quad (11)$$

By means of Eq. (11) the thermodynamic correction factor  $\xi$  is introduced, which basically equals the ratio of the probed volume and according ambient volume ( $\frac{V_2}{V_1}$ ) of air and which is used for the following discussions. Note that the temperature ratio included in  $\xi$  still depends on the air speeds  $v_1$  (TAS) and  $v_2$  (PAS). Insinuating an uncertainty of measured PAS of  $\pm 20\%$ , which is unrealistically high as resulting distortions in the particle images were highly visible (cf. Sect. 2.2 and Fig. 2), the resulting error of calculated  $T_2$  is at most  $\pm 3\%$  which influences the absolute effectiveness of  $\xi$  negligibly (cf. Sect. 3.2). Hence, with  $\xi$  the sensitivity of a correction factor to uncertainties in measured PAS is reduced, whereas the air speed ratio  $\frac{\text{PAS}}{\text{TAS}}$  is unabatedly affected by any uncertainty in measured PAS.

## Thermodynamic approach to correct for compression at Mach 0.7

R. Weigel et al.

Title Page

Abstract

Introduction

Conclusions

References

Tables

Figures

◀

▶

◀

▶

Back

Close

Full Screen / Esc

Printer-friendly Version

Interactive Discussion







similar to the CIPGs. In comparison to the CIPGs, the PIP setup features an increased detection volume covering larger particle sizes with  $100\mu\text{m} < D_p < 6400\mu\text{m}$ .

One major difference between CCP, NIXE-CAPS and PIP is the instrument-specific design of the probe heads. As shown in Fig. 5, CCP is equipped with a  $90^\circ$ -angled wedge. NIXE-CAPS combines a wedge of the same shape with an additional aerodynamic wingleet that may significantly contribute to the effective cross-sectional area of the NIXE-CAPS body. PIP is equipped with a half-sphere front cap. The different instrument heads have specific extension tips. Between the tips a free laser beam crosses the freely flowing sample air through which the particles pass. The sample area  $A_s$  of the probes, where the instrument is sensitive for particles crossing the open laser beam, is located almost half way between the tips.

One further important difference of the three instruments is their mounting position with respect to the aircraft fuselage (cf. Fig. 1b). PIP is mounted closest to the aircraft fuselage under the portside wing. NIXE-CAPS and CCP are positioned under the starboard wing on the intermediate and outbound hardpoints, respectively. Thus, with the three selected instruments the full range of available underwing probe positions with respect to the aircraft fuselage of HALO is covered.

### 3.2 Specific correction factor $\xi$ for HALO instruments

The continuous measurements of the parameters  $v_1$  (TAS),  $v_2$  (PAS),  $T_1$  (static air temperature),  $p_1$  (static ambient pressure) and  $p_2$  (static pressure at the probes) during flight allow for deriving the factors for the geometric correction  $\frac{PAS}{TAS}$  and the thermodynamic correction  $\xi$  as a function of TAS with 1 Hz temporal resolution. Hence, individual  $\xi$ -corrections are obtainable at any time during the measurement with pitot-equipped instruments. Figure 6 shows the comparison of calculated  $\xi$  and  $\frac{PAS}{TAS}$  corrections (synonymous for using TAS instead of PAS for  $N_{\text{meas}}$ , cf. Sect. 2.1) as a function of TAS. The unadjusted data from 6 out of a total of 11 ML-CIRRUS flights are shown. In sum, for the following, the 1 Hz-resolved data of more than 35 flight hours are treated.

## Thermodynamic approach to correct for compression at Mach 0.7

R. Weigel et al.

Title Page

Abstract

Introduction

Conclusions

References

Tables

Figures

◀

▶

◀

▶

Back

Close

Full Screen / Esc

Printer-friendly Version

Interactive Discussion



## Thermodynamic approach to correct for compression at Mach 0.7

R. Weigel et al.

Title Page

Abstract

Introduction

Conclusions

References

Tables

Figures

◀

▶

◀

▶

Back

Close

Full Screen / Esc

Printer-friendly Version

Interactive Discussion



During the flight on 29 March 2014 (red data points) the factors  $\frac{PAS}{TAS}$  and  $\xi$  as a function of TAS occasionally show significant deviation from the generally observed course. This deviation can unambiguously be apportioned to disturbed PAS measurements. The PAS chart is subject to disturbances either due to freezing conditions causing the pitot-tube to be tamped or due to non-isoaxial airflow caused by flight manoeuvres like tight turns. Very few and relatively short periods of PAS disturbances also occurred during the flight on 11 April 2014 (pink data points).

The  $\xi$ -correction is a monotonous function of flight velocity that has increasing effectiveness for each of the three instruments. Contrarily, the  $\frac{PAS}{TAS}$  correction appears to be systematically effective over the full range of air speeds, even at the lowest aircraft velocities – while the scatter of  $\frac{PAS}{TAS}$  by  $\sim 2$ – $10$  % may result from small scale turbulences or non-isoaxial airflow. However the geometric correction with  $\frac{PAS}{TAS}$  causes a general reduction of the values measured with CCP and NIXE-CAPS of not less than 20 %, even reaching 35 % for NIXE-CAPS (cf. Fig. 6). For CCP the values of  $\xi$  and  $\frac{PAS}{TAS}$  are most compact. The variability, in particular of  $\frac{PAS}{TAS}$ , increases for NIXE-CAPS over the complete TAS-range. For PIP the  $\xi$ -factor is comparably variable at flight velocities greater than  $140 \text{ m s}^{-1}$ . In comparison with the other probes the most severe differences were found for the correction factors of the PIP. Here, the geometric correction with  $\frac{PAS}{TAS}$  exhibits the highest effectiveness ( $\sim 20$  %) for lowest flight speeds and decreases with increasing velocities up to  $190 \text{ m s}^{-1}$  ( $\sim 10$  %). At a certain point ( $TAS \approx 190 \text{ m s}^{-1}$ ) the degree of correction with  $\frac{PAS}{TAS}$  takes a sharp turn and climbs again as higher air speeds are reached. For TAS-values greater than  $190 \text{ m s}^{-1}$  a correction with  $\frac{PAS}{TAS}$  would not strongly deviate from a correction made with corresponding  $\xi$ -factor.

The events when the pitot-tube was frozen or affected by misaligned inflow (mainly attributed to the measurements made on 29 March 2014 and to a limited number of measurements made on 11 April 2014) were removed from the data set which effectively reduces the data set volume by less than 3 %.

## Thermodynamic approach to correct for compression at Mach 0.7

R. Weigel et al.

Title Page

Abstract

Introduction

Conclusions

References

Tables

Figures

◀

▶

◀

▶

Back

Close

Full Screen / Esc

Printer-friendly Version

Interactive Discussion



For CCP measurements (data set as treated for Fig. 6) the parameters for calculating  $\xi$  according to Eq. (11) are shown in Fig. 7a as a function of TAS. Displayed are the absolute differences of measured pressures ( $p_1, p_2$ ) and velocities ( $v_1, v_2$ ). The difference of the squared velocities  $v_1$  and  $v_2$  (Eq. 11) is implicitly included in calculated  $T_2$ . Moreover the difference between measured temperature  $T_1$  and the calculated temperature  $T_2$  is shown. At a maximum TAS of  $255 \text{ ms}^{-1}$  the compression impact causes a  $\Delta v$  of up to  $75 \text{ ms}^{-1}$ , a  $\Delta T$  of up to 16 K and a  $\Delta p$  of about 30–60 hPa. In Fig. 7b the results of the pressure expression  $\frac{p_1}{p_2}$  (green data points) and temperature fraction  $\frac{T_2}{T_1}$  (black data points), as applied in Eq. (11), is displayed as a function of TAS, illustrating the respective effectiveness of each term to calculated  $\xi$ . The inversion to  $N_{\text{amb}}$  causes  $N_{\text{meas}}$  to be reduced by a factor of up to 0.8 to compensate for the induced pressure increase. In contrast, the compression-induced heating of air needs to be corrected by a factor of up to 1.07.

Remark: For a  $\text{TAS}_{\text{max}}$  of  $255 \text{ ms}^{-1}$  the compression-induced heating increases the temperature of the air sample by a  $\Delta T_{\text{max}}$  of 16 K. Assuming that the air gets compressed over a distance of  $\sim 0.5 \text{ m}$  upstream of the instrument (cf. Wendisch and Brenguier, 2013, Sect. 6.2.1 therein) then, for the given flight velocity, the airborne particles are exposed for an overall duration of about 2 ms to a continuously heating environment, ending up at the  $\Delta T_{\text{max}}$  of 16 K. The shrinkage of an airborne ice particle of  $2 \mu\text{m}$  initial size diameter is at most  $\sim 5\%$  after a 2 ms lasting exposure to a  $\Delta T_{\text{max}}$  of 16 K (at any initial air temperature of 190–245 K) at a static pressure of 300 hPa, as calculated from the mass rate change (Pruppacher and Klett, 2012; Spichtinger and Gierens, 2009). The shrinkage increases vigorously for particle of initial sub-micron size. Moreover, the compression of air over a distance of  $\sim 0.5 \text{ m}$  upstream of the instrument causes a  $\Delta p_{\text{max}}$  of 60 hPa (cf. Fig. 7a). If scaled to the dimensions of a droplet of millimetre-sized diameter (smaller particles are affected to lesser extent) the potential droplet deformation due to compression may be negligible.

In Fig. 8 the comparison of respectively measured  $p_2$  is shown together with the correlation of the PAS as derived from the dynamic pressure proportion of the pitot-tube

## Thermodynamic approach to correct for compression at Mach 0.7

R. Weigel et al.

Title Page

Abstract

Introduction

Conclusions

References

Tables

Figures

◀

▶

◀

▶

Back

Close

Full Screen / Esc

Printer-friendly Version

Interactive Discussion



measurements. The correlations of the individually measured  $p_2$  between NIXE-CAPS and CCP (Fig. 8, upper-left panel) and between PIP and CCP (Fig. 8, upper-right panel) agree almost in line with the displayed 1 : 1 relationship (dashed red lines). Thus, the  $p_2$  measurement of the instruments does not seem to be significantly affected, neither by the individual probe head design nor by the respective wing position. Note that the calibrated pressure transducers commonly integrated in the individual probes are of the type Honeywell, model 142PC15A with a specified linearity within  $\pm 0.4\%$  of the output signal span for the pressure range between 140 and 1030 hPa. When comparing the PAS obtained from the individual instruments a feature sticks out that seems to solely result from influences on the dynamic pressure from measurements with the pitot-tube.

The dynamic pressure for calculating the air speed results from the total pressure, impacting on the pitot's forward facing congestion tube, subtracted by the static pressure that is detected at the pitot-tube's flanks. Hence, the PAS comparison between NIXE-CAPS and CCP (Fig. 8, lower-left panel) exhibits a systematic discrepancy of about  $5\text{--}10\text{ ms}^{-1}$  by which the resulting PAS of the CCP exceeds the NIXE-CAPS measurements over the entire velocity range. This may result from different calibrations of the respective pitot-tube or it could be an effect of the instrument's wing position. It is also likely that the systematically stronger deceleration of air flow upstream of NIXE-CAPS is caused by its winglet (cf. Fig. 5) which may increase the probe's cross-sectional-area compared to that of the CCP. Apparently the PAS measured by the PIP increasingly deviates from the CCP-PAS as a function of flight speed. Therefore, the deviation is not of a constant character, but rather increases with increasing flight speed. This shows that the extraordinary behaviour of  $\frac{\text{PAS}}{\text{TAS}}$  over the range of flight velocity (cf. Fig. 6, right panel) is only connected to the dynamic pressure proportion obtained from the PIP's pitot-tube measurements. Unless the PIP could be deployed at another HALO underwing position, at least for one flight for investigating this issue more closely, it appear conceivable that the effect originates from an external interference due the PIP's proximity either to the wing root or to the fuselage of HALO. For comparably much smaller flight velocities ( $< 100\text{ ms}^{-1}$ ) previous studies demonstrated that the air flow field changes along the

wing span with different impact on instruments positioned outboard or inboard at an aircraft's wing (Drummond and MacPherson, 1985; MacPherson and Baumgardner, 1988).

For providing a parameterisation of  $\xi$ -values as a function of TAS the data set needs to be reassessed by accounting for the limited periods of tamped or malfunctioning pitot-tubes. For the following, those periods that were identified to be affected by an inoperative pitot-tube have been removed from the data set. In Fig. 9 the derived  $\xi$ -factor is depicted as a function of TAS. The parameterisation results from fitting a quadratic regression (Table 1) to the given data set. For each instrument the individually derived parameters of  $v_2$  (PAS), and  $p_2$  (static air pressure at the probe) are used, such that the  $\xi$ -factors are also individually determined for each instrument. The regression fits in Fig. 9 are provided together with the 95 %-confidence band (blue lines) and the 95 %-prediction band (red lines). Note, that the 95 %-confidence band is very narrow, even covering the black regression fit because the data set used for these regressions is large and the data variability is small. The fit parameters are summarised in Table 1 and the regressions generally reveal values of  $r^2$  greater than 0.95, which confirms the solidity of the functional relationship between  $\xi$  and TAS.

### 3.3 The consistency of $\xi$ for HALO instruments

Further insight into the properties of  $\xi$  is provided by Fig. 10 that illustrates the correlation of individually derived  $\xi$ -values for each instrument. The  $\xi$ -data are color-coded according to TAS and the linear correlation between the instrument-specific  $\xi$ -data and TAS are derived. The graphs also contain the very narrow 95 %-confidence band (blue lines) and the 95 %-prediction band (red lines). The parameters for the linear correlations shown in Fig. 10 are also summarised in Table 1. Generally the  $\xi$ -values exhibit a strong correlation with a correlation coefficient  $r^2$  larger than 0.97, which indicates  $\xi$  to be widely independent of the instrument characteristics, such as wing position or design, in contrast to  $\frac{PAS}{TAS}$ . Nevertheless, in detail the individual  $\xi$ -values obviously differ from each other, which is presumably connected to the differently shaped probe

## Thermodynamic approach to correct for compression at Mach 0.7

R. Weigel et al.

Title Page

Abstract

Introduction

Conclusions

References

Tables

Figures

◀

▶

◀

▶

Back

Close

Full Screen / Esc

Printer-friendly Version

Interactive Discussion











## Thermodynamic approach to correct for compression at Mach 0.7

R. Weigel et al.

Title Page

Abstract

Introduction

Conclusions

References

Tables

Figures

◀

▶

◀

▶

Back

Close

Full Screen / Esc

Printer-friendly Version

Interactive Discussion



of air due to the moving instrument body and the compression-induced motion of particles out of their ambient (undisturbed) state is ignored. As a consequence of the compression upstream of a probe, the air speed (PAS) and the particle speed at the point of measurement must be systematically lower compared to TAS. Determining particle number concentrations by using the TAS without adjustments regarding the compression leads to an underrepresentation of particle concentrations that is not negligible.

- b. The measured particle number concentration  $N_{\text{meas}}$  (based on the recorded PAS, cf. Paragraph 2.1 for details) does not represent the ambient number concentration of cloud particles. The compression of air causes a modification of the particle's environment and behaviour at the point of measurement compared to ambient (undisturbed) conditions. Thus, the measured particle number concentrations without any corrections may be representative for the measurement conditions only. However, compared to ambient particle number concentrations, the uncorrected  $N_{\text{meas}}$  is an overestimate of increasing strength with flight velocity. Note that an uncertainty of  $N_{\text{meas}}$  remains due to the PAS uncertainty which may not considerably exceed 10 %.
- c. Multiplying measured particle number concentrations  $N_{\text{meas}}$  with the ratio  $\frac{\text{PAS}}{\text{TAS}}$ , as practiced, with the attempt to hereby invert the measured concentrations to ambient conditions lacks any physical rationale. The ratio of air speeds does not account for the compression of air upstream of the probe which is the major reason for the deviation of measured air speeds, PAS and TAS. By using the ratio  $\frac{\text{PAS}}{\text{TAS}}$ , the increase of pressure and the heating accompanied with the compression of air remains fully ignored. Hence, this simplified correction procedure turns out to cause an unreasonable reduction of particle number concentrations. This procedure was shown to affect the results at surprisingly low aircraft speeds. Contrarily, the impact of this procedure was demonstrated to depend on the instruments' underwing position with respect to the aircraft fuselage.





## References

- Baumgardner, D., Strapp, W., and Dye, J. E.: Evaluation of the forward scattering spectrometer probe. Part II: Corrections for coincidence and dead-time losses, *J. Atmos. Ocean. Tech.*, 2, 626–632, doi:10.1175/1520-0426(1985)002<0626:eotfss>2.0.co;2, 1985.
- 5 Baumgardner, D., Jonsson, H., Dawson, W., O'Connor, D., and Newton, R.: The cloud, aerosol and precipitation spectrometer: a new instrument for cloud investigations, *Atmos. Res.*, 59–60, 251–264, doi:10.1016/S0169-8095(01)00119-3, 2001.
- Baumgardner, D., Brenguier, J. L., Bucholtz, A., Coe, H., DeMott, P., Garrett, T. J., Gayet, J. F., Hermann, M., Heymsfield, A., Korolev, A., Krämer, M., Petzold, A., Strapp, W., Pilewskie, P., Taylor, J., Twohy, C., Wendisch, M., Bachalo, W., and Chuang, P.: Airborne instruments to measure atmospheric aerosol particles, clouds and radiation: a cook's tour of mature and emerging technology, *Atmos. Res.*, 102, 10–29, doi:10.1016/j.atmosres.2011.06.021, 2011.
- 10 Baumgardner, D., Newton, R., Krämer, M., Meyer, J., Beyer, A., Wendisch, M., and Vochezer, P.: The Cloud Particle Spectrometer with Polarization Detection (CPSPD): a next generation open-path cloud probe for distinguishing liquid cloud droplets from ice crystals, *Atmos. Res.*, 142, 2–14, doi:10.1016/j.atmosres.2013.12.010, 2014.
- Dixon, J. C.: Appendix B: properties of air, in: *The Shock Absorber Handbook*, John Wiley & Sons LTD, Chichester, UK, 375–378, 2007.
- Drummond, A. M. and MacPherson, J. I.: Aircraft flow effects on cloud drop images and concentrations measured by the NAE twin otter, *J. Atmos. Ocean. Tech.*, 2, 633–643, doi:10.1175/1520-0426(1985)002<0633:afeocd>2.0.co;2, 1985.
- 20 Dye, J. E. and Baumgardner, D.: Evaluation of the forward scattering spectrometer probe. Part I: Electronic and optical studies, *J. Atmos. Ocean. Tech.*, 1, 329–344, doi:10.1175/1520-0426(1984)001<0329:eotfss>2.0.co;2, 1984.
- 25 Finger, F., Werner, F., Klingebiel, M., Ehrlich, A., Jäkel, E., Voigt, M., Borrmann, S., Spichtinger, P., and Wendisch, M.: Spectral optical layer properties of cirrus from collocated airborne measurements – a feasibility study, *Atmos. Chem. Phys. Discuss.*, 15, 19045–19077, doi:10.5194/acpd-15-19045-2015, 2015.
- 30 Frey, W., Eichler, H., de Reus, M., Maser, R., Wendisch, M., and Borrmann, S.: A new airborne tandem platform for collocated measurements of microphysical cloud and radiation properties, *Atmos. Meas. Tech.*, 2, 147–158, doi:10.5194/amt-2-147-2009, 2009.

### Thermodynamic approach to correct for compression at Mach 0.7

R. Weigel et al.

Title Page

Abstract

Introduction

Conclusions

References

Tables

Figures



Back

Close

Full Screen / Esc

Printer-friendly Version

Interactive Discussion



## Thermodynamic approach to correct for compression at Mach 0.7

R. Weigel et al.

Title Page

Abstract

Introduction

Conclusions

References

Tables

Figures

◀

▶

◀

▶

Back

Close

Full Screen / Esc

Printer-friendly Version

Interactive Discussion



Frey, W., Borrmann, S., Kunkel, D., Weigel, R., de Reus, M., Schlager, H., Roiger, A., Voigt, C., Hoor, P., Curtius, J., Krämer, M., Schiller, C., Volk, C. M., Homan, C. D., Fierli, F., Di Donfrancesco, G., Ulanovsky, A., Ravegnani, F., Sitnikov, N. M., Viciani, S., D'Amato, F., Shur, G. N., Belyaev, G. V., Law, K. S., and Cairo, F.: In situ measurements of tropical cloud properties in the West African Monsoon: upper tropospheric ice clouds, Mesoscale Convective System outflow, and subvisual cirrus, *Atmos. Chem. Phys.*, 11, 5569–5590, doi:10.5194/acp-11-5569-2011, 2011.

Hinds, W. C.: *Aerosol Technology: Properties, Behavior, and Measurement of Airborne Particles* (2nd edition), John Wiley & Sons LTD, Chichester, UK, 1999.

Kärcher, B. and Lohmann, U.: A parameterization of cirrus cloud formation: Homogeneous freezing of supercooled aerosols, *J. Geophys. Res.-Atmos.*, 107, 4010, doi:10.1029/2001jd000470, 2002.

Klingebiel, M., de Lozar, A., Molleker, S., Weigel, R., Roth, A., Schmidt, L., Meyer, J., Ehrlich, A., Neuber, R., Wendisch, M., and Borrmann, S.: Arctic low-level boundary layer clouds: in situ measurements and simulations of mono- and bimodal supercooled droplet size distributions at the top layer of liquid phase clouds, *Atmos. Chem. Phys.*, 15, 617–631, doi:10.5194/acp-15-617-2015, 2015.

Knollenberg, R. G.: The optical array: an alternative to scattering or extinction for airborne particle size determination, *J. Appl. Meteorol.*, 9, 86–103, doi:10.1175/1520-0450(1970)009<0086:toaat>2.0.co;2, 1970.

Korolev, A.: Reconstruction of the sizes of spherical particles from their shadow images. Part I: Theoretical considerations, *J. Atmos. Ocean. Tech.*, 24, 376–389, doi:10.1175/jtech1980.1, 2007.

Korolev, A., Makarov, Y. E., and Novikov, V.: On the calibration of photoelectric cloud droplet spectrometer FSSP-100, *TCAO*, 158, 43–49, 1985.

Korolev, A. V., Kuznetsov, S. V., Makarov, Y. E., and Novikov, V. S.: Evaluation of measurements of particle size and sample area from optical array probes, *J. Atmos. Ocean. Tech.*, 8, 514–522, doi:10.1175/1520-0426(1991)008<0514:eomops>2.0.co;2, 1991.

Korolev, A. V., Strapp, J. W., and Isaac, G. A.: Evaluation of the accuracy of PMS optical array probes, *J. Atmos. Ocean. Tech.*, 15, 708–720, doi:10.1175/1520-0426(1998)015<0708:eotaop>2.0.co;2, 1998.

Krämer, M., Schiller, C., Afchine, A., Bauer, R., Gensch, I., Mangold, A., Schlicht, S., Spelten, N., Sitnikov, N., Borrmann, S., de Reus, M., and Spichtinger, P.: Ice supersaturations



## Thermodynamic approach to correct for compression at Mach 0.7

R. Weigel et al.

Title Page

Abstract

Introduction

Conclusions

References

Tables

Figures

◀

▶

◀

▶

Back

Close

Full Screen / Esc

Printer-friendly Version

Interactive Discussion



Voigt, C., Schumann, U., Minikin, A., and Team, A.: ML-CIRRUS – the airborne experiment on natural cirrus and contrail-cirrus with the new 1 High Altitude Long range research aircraft HALO, B. Am. Meteorol. Soc., BAMS-D-15–00213, 2015.

Wendisch, M. and Brenguier, J.-L.: Airborne measurements for Environmental Research: Methods and Instruments, John Wiley & Sons LTD, Chichester, UK, 2013.

Wendisch, M., Pöschl, U., Andreae, M. O., Machado, L. A. T., Albrecht, R., Schlager, H., Rosenfeld, D., Martin, S. T., Abdelmonem, A., Afchine, A., Araùjo, A., Artaxo, P., Aufmhoff, H., Barbosa, H. M. J., Borrmann, S., Braga, R., Buchholz, B., Cecchini, M. A., Costa, A., Curtius, J., Dollner, M., Dorf, M., Dreiling, V., Ebert, V., Ehrlich, A., Ewald, F., Fisch, G., Fix, A., Frank, F., Fütterer, D., Heckl, C., Heidelberg, F., Hüneke, T., Jäkel, E., Järvinen, E., Jurkat, T., Kanter, S., Kästner, U., Kenntner, M., Kesselmeier, J., Klimach, T., Knecht, M., Kohl, R., Kölling, T., Krämer, M., Krüger, M., Krisna, T. C., Lavric, J. V., Longo, K., Mahnke, C., Manzi, A. O., Mayer, B., Mertes, S., Minikin, A., Molleker, S., Münch, S., Nillius, B., Pfeilsticker, K., Pöhlker, C., Roiger, A., Rose, D., Rosenow, D., Sauer, D., Schnaiter, M., Schneider, J., Schulz, C., de Souza, R. A. F., Spanu, A., Stock, P., Vila, D., Voigt, C., Walser, A., Walter, D., Weigel, R., Weinzierl, B., Werner, F., Yamasoe, M. A., Ziereis, H., Zinner, T., and Zöger, M.: Introduction of the ACRIDICON–CHUVA campaign studying deep convective clouds and precipitation over Amazonia using the new German HALO research aircraft, BAMS-D-14-00255, B. Am. Meteorol. Soc., submitted, 2015.

Willeke, K. and Baron, P. A.: Aerosol measurement, Principles, Techniques and Applications, Van, John Wiley & Sons LTD, Chichester, UK, 1993.



## Thermodynamic approach to correct for compression at Mach 0.7

R. Weigel et al.

**Table 2.** Altitude and flight velocity for the ACRIDICON-CHUVA mission flight “AC13” on 19 September 2014 over the time period between 20:00:40 UTC (72 040 s of day) and 20:32:00 UTC (73 920 s of day) and derived corrections of  $\xi$  and  $\frac{PAS}{TAS}$  for CCP and PIP.

	flight altitude in m.a.s.l.	TAS in $\text{ms}^{-1}$	$\xi$ – CCP	$\xi$ – PIP	$\frac{PAS}{TAS}$ – CCP	$\frac{PAS}{TAS}$ – PIP
Average	12 971.6	221.75	0.90	0.87	0.73	0.89
Maximum	12 980.7	226.89	0.91	0.87	0.74	0.90
Minimum	12 962.5	215.12	0.89	0.86	0.72	0.88

[Title Page](#)
[Abstract](#)
[Introduction](#)
[Conclusions](#)
[References](#)
[Tables](#)
[Figures](#)
[Back](#)
[Close](#)
[Full Screen / Esc](#)
[Printer-friendly Version](#)
[Interactive Discussion](#)


## Thermodynamic approach to correct for compression at Mach 0.7

R. Weigel et al.

Title Page

Abstract

Introduction

Conclusions

References

Tables

Figures

⏪

⏩

◀

▶

Back

Close

Full Screen / Esc

Printer-friendly Version

Interactive Discussion



**Table 3.** Coefficients of the statistical analyses of derived  $\xi$ -values for CCP measurements on the Learjet-35A: quadratic regression with parameters and standard deviations ( $\sigma$ ). The  $\xi$ -parameterisation is based on > 12 000 single 1 Hz-data points ( $\approx$  3.3 flight hours).

Regression for parameterisation of $\xi$ as a function of Learjet-TAS: cf. Table 1	
CCP	
$y_0 \pm \sigma$	$0.99 \pm 6.91 \times 10^{-4}$
$a \pm \sigma$	$3.74 \times 10^{-4} \pm 8.35 \times 10^{-6}$
$b \pm \sigma$	$-3.08 \times 10^{-6} \pm 2.48 \times 10^{-8}$
$r^2$	0.97

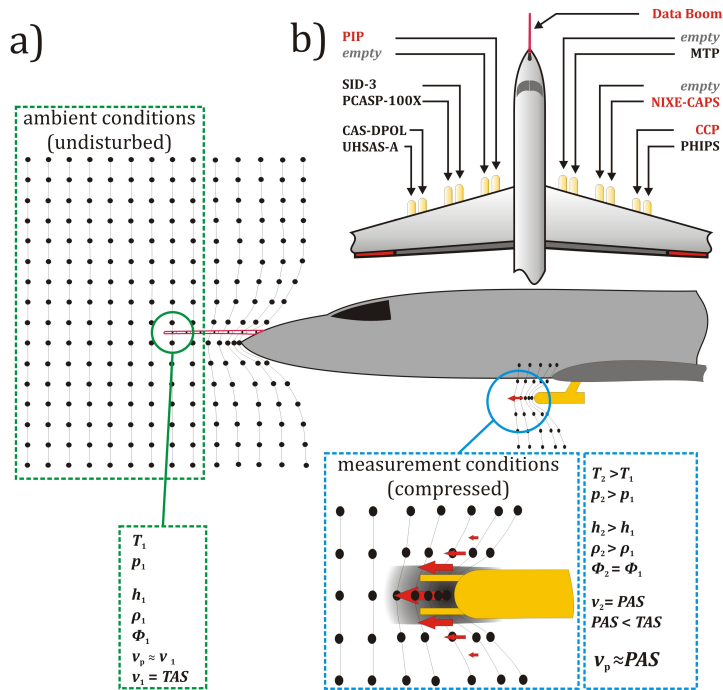


**Figure 1.** Illustration of the aircraft geometry, different types of probes and their underlying position, and air compression effects. **(a)** The moving aircraft induces an increase of particle concentration in particular upstream of the underlying probes (grey-shaded area). Parameters used for deriving a thermodynamic correction are listed for ambient (undisturbed) conditions (green box) and for measurement conditions (blue box). Note that specified velocities refer to the moving aircraft or instrument relative to the air or the particles. **(b)** The top-view diagram of the aircraft indicates the probe's mounting position during the ML-CIRRUS and the ACRIDICON-CHUVA field missions. Data originating from the probes indicated in red are used for this study. (Instrument name acronyms are specified in the text).

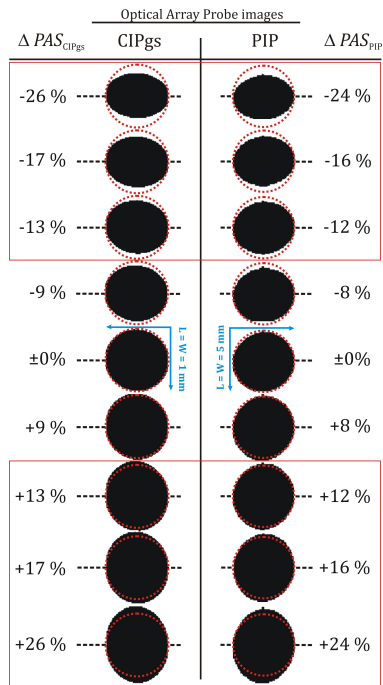


**Figure 2.** Shadow cast images of non-transparent circular spots on a spinning disk (for calibration purposes) passing the probes' sample area  $A_s$  with constant velocity ( $\sim 23\text{--}25 \text{ m s}^{-1}$ ). For this illustration, in the data acquisition program, the air speed (PAS) is manually varied stepwise with the finest available resolution for triggering the timing of imaging. Manually shifting the PAS causes a positive or a negative deviation ( $\Delta PAS$ ) of the air speed relative to the constant disk rotation speed  $v_{rot}$ . Deformed images relative to the dashed red circles of identical diameter (according to  $\Delta PAS = \pm 0\%$  if  $v_{rot} = PAS$ , marked in blue) indicate image distortion that becomes significant for  $\Delta PAS$  exceeding 10% (red boxes). PIP images are slightly shifted as  $v_{rot}$  of two radially opposed points on the edges of a 5 mm-sized disk spot increases with distance from the disk's centre.

## Thermodynamic approach to correct for compression at Mach 0.7

R. Weigel et al.

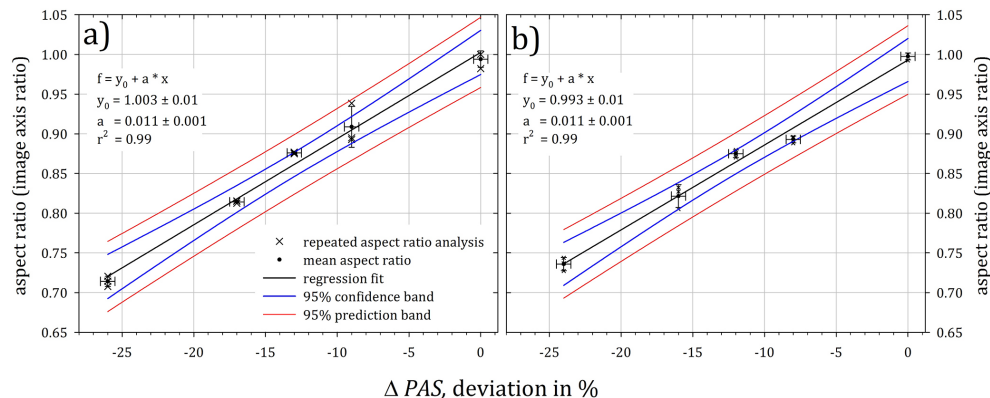


**Figure 3.** Aspect ratios of taken images as a function of the deviation of the Probe Air Speed (PAS) from the penetration speed of a circular object through the instrument's detection region. The image aspect ratio provides a measure of the distortion strength when the PAS setting is manually shifted in the data acquisition software compared to the constant penetration speed of a circular object on the spinning disc used for calibrations of an Optical Array Probe (OAP). **(a)** for the Cloud Combination Probe's CIP and **(b)** for the Precipitation Imaging Probe (PIP).

Title Page

Abstract

Introduction

Conclusions

References

Tables

Figures

◀

▶

◀

▶

Back

Close

Full Screen / Esc

Printer-friendly Version

Interactive Discussion



## Thermodynamic approach to correct for compression at Mach 0.7

R. Weigel et al.

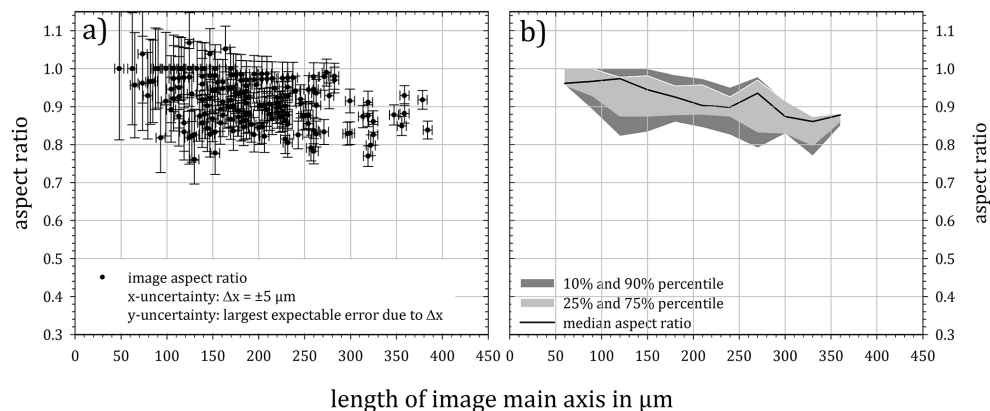


**Figure 4.** Aspect ratios as a function of the image’s main axis dimension as revealed from reanalysis of more than 200 particle images acquired over  $\sim 6$  flight hours during the ACRIDICON-CHUVA mission flight “AC13” on 19 September 2014, over the Amazonian basin, Brazil. Random samples, exclusively of images that indicate to originate from spheroidal objects, were taken well distributed over the data sets recorded during the complete flight. Images of spheroidal objects exhibit particular symmetry and shading intensity compared to other particle species. Flight speeds covered:  $\sim 41\%$  of the flight at  $200\text{--}220 \text{ms}^{-1}$ ,  $\sim 16\%$  at  $140\text{--}180 \text{ms}^{-1}$ ,  $\sim 25\%$  at  $120\text{--}140 \text{ms}^{-1}$ ,  $\sim 18\%$  ascents and descents with various flight speeds. **(a)** The measured aspect ratio of the individual images of spheroidal particles, and **(b)** the statistically treated data provided as median of the aspect ratios together with 10%-, 25%-, 75%-, 90%-percentiles.

[Title Page](#)
[Abstract](#)
[Introduction](#)
[Conclusions](#)
[References](#)
[Tables](#)
[Figures](#)
[◀](#)
[▶](#)
[◀](#)
[▶](#)
[Back](#)
[Close](#)
[Full Screen / Esc](#)
[Printer-friendly Version](#)
[Interactive Discussion](#)


## Thermodynamic approach to correct for compression at Mach 0.7

R. Weigel et al.

Title Page

Abstract

Introduction

Conclusions

References

Tables

Figures

◀

▶

◀

▶

Back

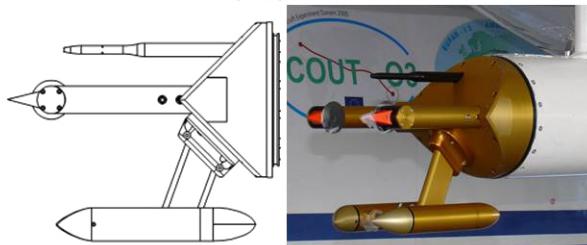
Close

Full Screen / Esc

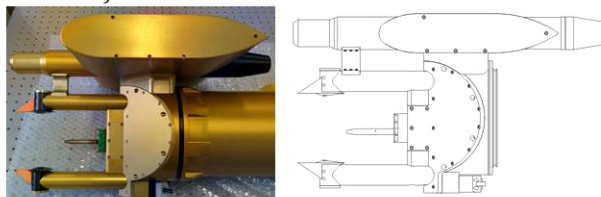
Printer-friendly Version

Interactive Discussion

Cloud Combination Probe (CCP)



Novel Ice eXperiment - Cloud, Aerosol and Precipitation Spectrometer (NIXE-CAPS)



Precipitation Imaging Probe (PIP)

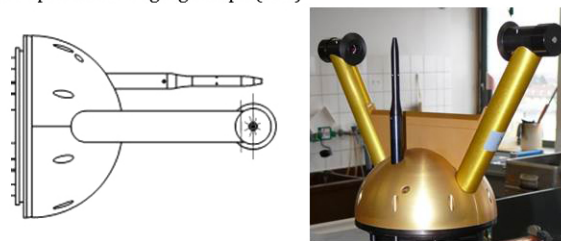


**Figure 5.** Diagrams and images of the different instrument heads of quasi-streamlined design. Top: Cloud Combination Probe (CCP) with 90°-angled wedge. Middle: combined probe head of 90°-angled wedge and additional winglet of NIXE-CAPS. Bottom: Precipitation Imaging Probe (PIP) with half-sphere probe head.

## Thermodynamic approach to correct for compression at Mach 0.7

R. Weigel et al.

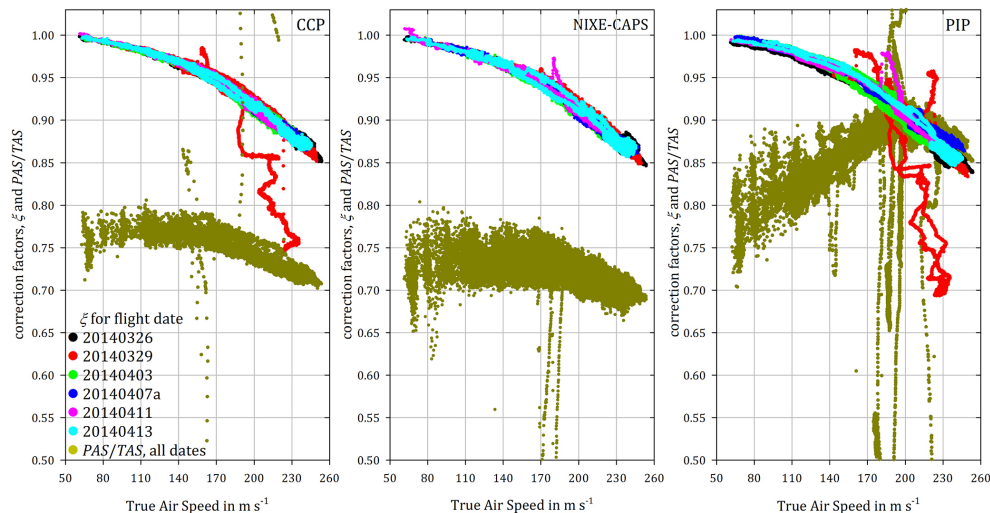


**Figure 6.** Comparison of two different instrument-specific corrections applied to data acquired on HALO during ML-CIRRUS. The geometric correction  $\frac{PAS}{TAS}$  causes a general downscaling of measured concentrations of 20 % to up to 35 % for NIXE-CAPS and CCP. Thereby  $\frac{PAS}{TAS}$  is highly variable, ambiguous and shows significant dependence on the instrument's wing position. At the PIP position (portside, innermost) the behaviour of  $\frac{PAS}{TAS}$  as a function of TAS is different, presumably due to air flow disturbances by the aircraft's fuselage. Instrument-specific  $\xi$ -values exhibits higher compactness over the TAS-range and show reduced dependence on the wing position. The data are from six ML-CIRRUS flights and include outliers due to freezing of the pitot-tubes or due to distortions from isoaxial flow accompanied with manoeuvres such as tight turns.

Title Page

Abstract

Introduction

Conclusions

References

Tables

Figures

◀

▶

◀

▶

Back

Close

Full Screen / Esc

Printer-friendly Version

Interactive Discussion



**Thermodynamic approach to correct for compression at Mach 0.7**

R. Weigel et al.

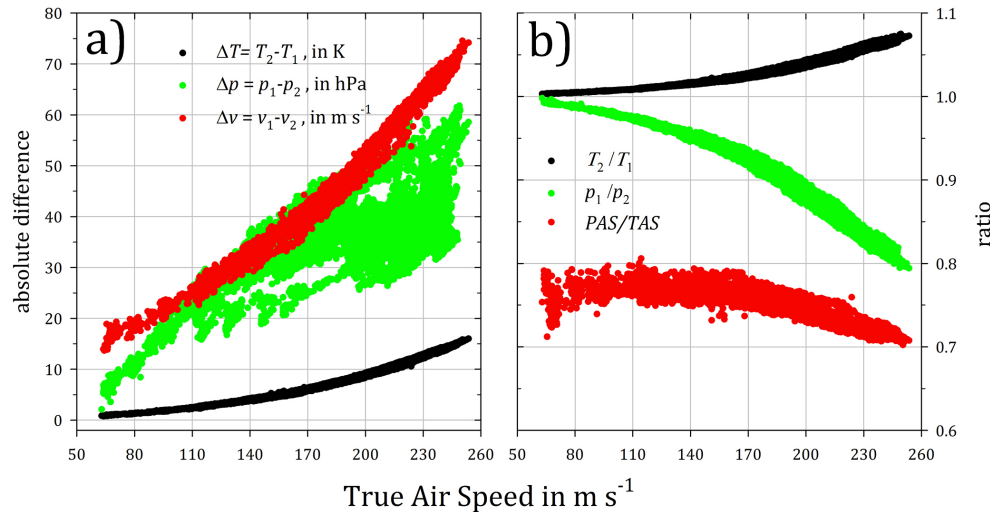


**Figure 7.** Relevant parameters for determining  $\xi$  as a function of TAS for the CCP. **(a)** The absolute difference of measured pressures ( $p_1$ ,  $p_2$ ) and velocities ( $v_1$ ,  $v_2$ ) and the difference of measured temperature  $T_1$  to calculated  $T_2$ . **(b)** The ratio of pressures  $\frac{p_1}{p_2}$  and temperatures  $\frac{T_2}{T_1}$  as used in Eq. (11) to illustrate respective effectiveness in the  $\xi$ -correction.

Title Page

Abstract Introduction

Conclusions References

Tables Figures

◀ ▶

◀ ▶

Back Close

Full Screen / Esc

Printer-friendly Version

Interactive Discussion



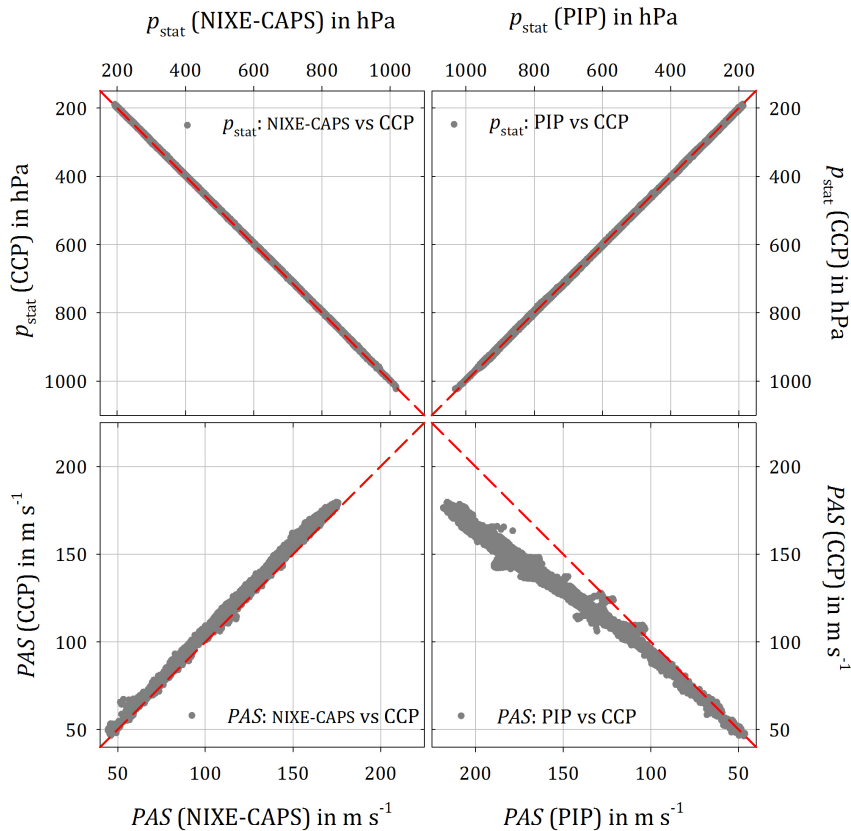


**Figure 8.** Correlations between individually measured static pressures and PAS for each instrument pair. The  $p$  correlations (upper panels) indicate consistency as the data follow the 1 : 1 relationship (dashed red lines). The PAS-correlations (lower panels) reveal systematic deviations from the 1 : 1 relationship, indicative for an unspecified flow disturbance at according instrument position.

**Thermodynamic approach to correct for compression at Mach 0.7**

R. Weigel et al.

Title Page

Abstract

Introduction

Conclusions

References

Tables

Figures

◀

▶

◀

▶

Back

Close

Full Screen / Esc

Printer-friendly Version

Interactive Discussion





## Thermodynamic approach to correct for compression at Mach 0.7

R. Weigel et al.

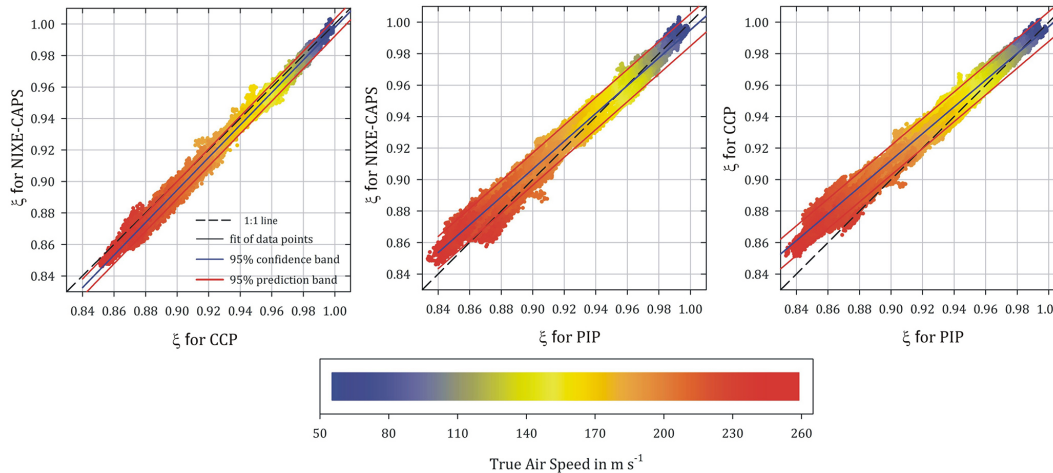


**Figure 10.** Correlations of instrument-specific  $\xi$ . The deviation from the 1:1 relationship (dashed black lines) as a function of the aircraft True Air Speed (TAS) is strongest at the PIP position (portside, innermost). Coefficients for the correlations are provided in Table 1.

Title Page

Abstract

Introduction

Conclusions

References

Tables

Figures

◀

▶

◀

▶

Back

Close

Full Screen / Esc

Printer-friendly Version

Interactive Discussion



## Thermodynamic approach to correct for compression at Mach 0.7

R. Weigel et al.

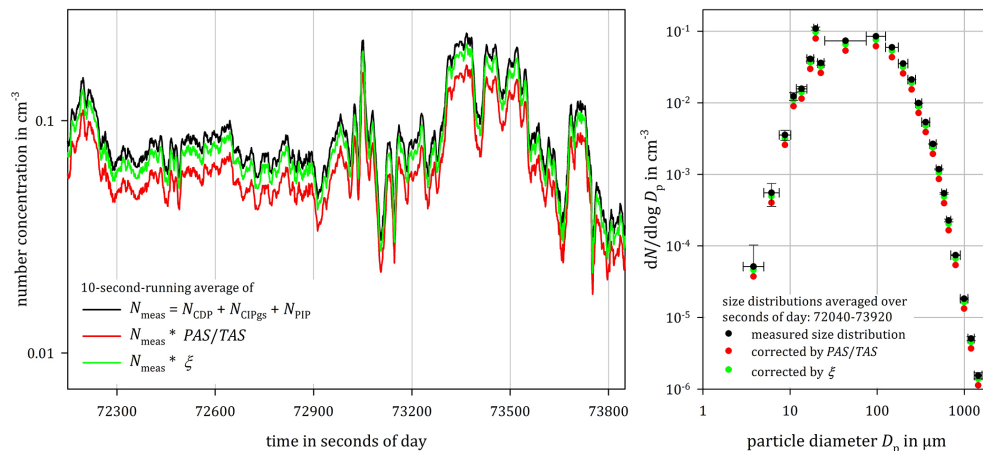


**Figure 11.** Resulting particle number concentration after application of different correction procedures on data acquired during the ACRIDICON-CHUVA mission flight “AC13” on 19 September 2014 between 20:00:40 UTC (72 040 s of day) and 20:32:00 UTC (73 920 s of day), over the Amazonian basin, Brazil. Left panel: the time series of total particle concentration measured with CCP and PIP. Right panel: the resulting particle size distribution, merged from CCP (CDP and CIPgs) and PIP measurements.

Title Page

Abstract

Introduction

Conclusions

References

Tables

Figures



Back

Close

Full Screen / Esc

Printer-friendly Version

Interactive Discussion



## Thermodynamic approach to correct for compression at Mach 0.7

R. Weigel et al.

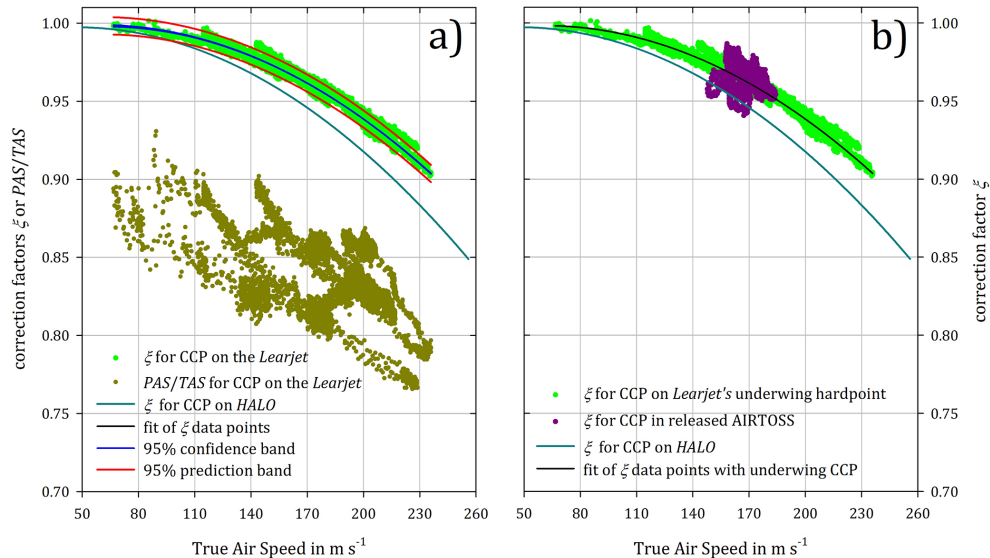


**Figure 12.** Comparison of corrections for the CCP **(a)** with the CCP attached to a Learjet-35A's underwing hardpoint (flight on 5 September 2013) during the AIRTOSS-ICE mission over Northern Germany. The  $\frac{\text{PAS}}{\text{TAS}}$  correction exhibits broad scatter and ambiguities. Instead, the determined  $\xi$ -values yield compactness over the complete TAS-range. For comparison the  $\xi$ -parameterisation from HALO measurements of the CCP are implied, illustrating the dependence of  $\xi$  on the used measurement platform. **(b)** instead of  $\frac{\text{PAS}}{\text{TAS}}$  the  $\xi$ -values are shown for the CCP when deployed in the AIRcraft Towed Sensor Shuttle (AIRTOSS) released from the Learjet-35A on a steel cable.